Materials Letters 411 (2026) 140326

Contents lists available at ScienceDirect

Materials Letters

journal homepage: www.elsevier.com/locate/matlet

Improved corrosive wear behavior of $Al_2O_3/MoS_2/La_2P_4O_{13}$ composite layer in-situ prepared by micro arc oxidation

Tao Liu [a], Jian Shang [a,*], Qian Li [b]

[a] School of Materials Science and Engineering, Liaoning University of Technology, Jinzhou 121001, China
[b] Shandong Innovation Metal Technology Co, Binzhou 256600, China

ARTICLE INFO

Keywords:
Aluminum alloy
Micro-arc oxidation
Microstructure and properties
Corrosive wear

ABSTRACT

In this study, Al_2O_3/MoS_2 and $Al_2O_3/MoS_2/La_2P_4O_{13}$ composite layers were in-situ prepared on 6082-T6 alloy via micro-arc oxidation (MAO). Their microstructure, as well as the wear behavior in 3.5% NaCl corrosive solution and air, were investigated comparatively, and electrochemical corrosion tests were also conducted. Compare with the Al_2O_3/MoS_2 layer (hardness: 737 HV_1; average friction coefficient: 0.543; wear rate: 4.138 × 10^{-6} $mm^3/N{\cdot}m$), the $Al_2O_3/MoS_2/La_2P_4O_{13}$ layer's hardness is elevated by 65% to 1236 HV_1, friction coefficient drops to 0.350, and wear rate is reduced by two orders of magnitude to 9.5 × 10^{-8} $mm^3/N{\cdot}m$. Electrochemical tests showed that lanthanum acetate caused a positive potential shift and negative corrosion current shift, The La^{3+} enables in-situ formation at Al_2O_3/Al_2O_3 interfaces. LaP_xO_y and MoS_2 show lubricating/inhibiting effects and make the layer more dense. This contributes to simultaneous high wear and corrosion resistance.

1. Introduction

The 6082-T6 alloy is extensively used for lightweight automotive components, marine structural parts, and aerospace precision components [1–3] because of its high strength, good toughness, and other excellent mechanical properties. However, the alloy is susceptible to wear, particularly in humid or corrosive environments, owing to its low surface hardness. Therefore, further applications in demanding service conditions involving heavy loads or harsh serving environments are constrained. MAO is an efficient surface modification technique that enables the in-situ growth of a strongly bonded ceramic layer on valve metal or alloy surfaces. Composite layers can be prepared in situ by regulating the composition of the electrolyte and working parameters to enhance wear and corrosion resistance [4–6]. Relevant studies have shown that incorporating functional additives or particles can optimize the surface properties of Al alloy [7,8]. MoS_2, because of its outstanding lubricating properties is often taken as the adding component into the layer to reduce the coefficient of friction [9–11]. Lanthanum phosphate exhibits favorable thermal stability at elevated temperatures. Morgan et al. [12] found that $Al_2O_3/LaPO_4$ composites are nearly insoluble in both acids and alkalis.

In this study, considering the lubricating function of MoS_2 and stability of $La_2P_4O_{13}$, Al_2O_3/MoS_2 and $Al_2O_3/MoS_2/La_2P_4O_{13}$ composite layers are in-situ prepared by MAO method on 6082-T6 alloy through addition of $C_2H_6LaO_3$ into the electrolyte. The microstructure, hardness and corrosive wear behavior in 3.5% NaCl corrosive solution of two composite layers are investigated. This study can provide a new layer design route to improve wear and corrosion resistance simultaneously.

2. Experiment

2.1. Materials and experimental parameters

The 6082-T6 aluminum alloy substrate, sized 25 mm × 25 mm × 3 mm, was polished with sandpaper, ultrasonically cleaned with alcohol, and treated to remove oil and oxide layers with 2% HF and 50 g/L NaOH, respectively. Composite layers were prepared using a WHD-30 apparatus with a current density of 11 A/dm^2, frequency of 500 Hz, oxidation time of 20 min, and duty cycle of 30%. The electrolyte is composed of 15 g/L $(NaPO_3)_6$ + 5 g/L Na_2MoO_4 + 10 g/L Na_2S + (0, 5 g/L) $C_2H_6LaO_3$ + 10 g/L EDTA.

2.2. Preparation and characterization

Al alloy specimens were suspended from an anode rod and immersed in an electrolyte solution cooled to 30 °C. $C_2H_6LaO_3$ was added to

* Corresponding author.
E-mail address: shangbahao@163.com (J. Shang).

https://doi.org/10.1016/j.matlet.2026.140326
Received 12 January 2026; Accepted 21 February 2026
Available online 23 February 2026

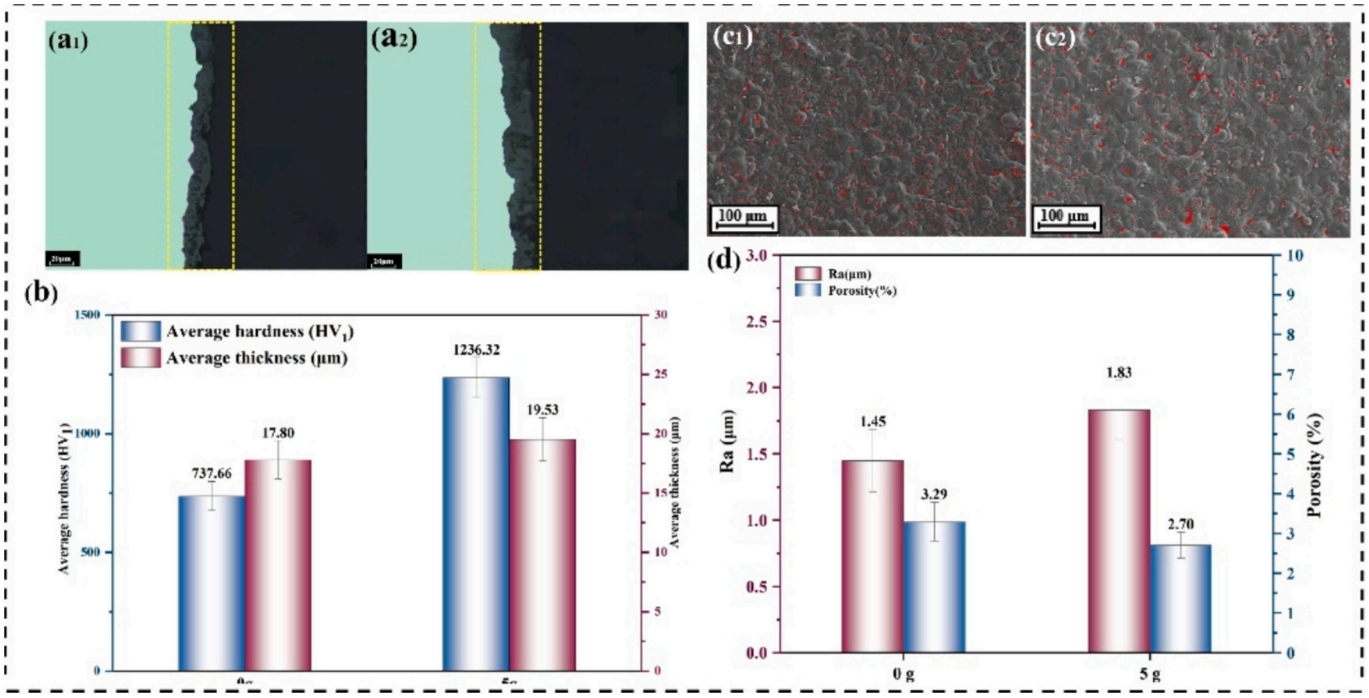

Fig. 1. (a_1, a_2): Metallographic images of composite layer cross-sections with 0 and 5 g/L lanthanum acetate; (b): Histograms of hardness, thickness;(c_1, c_2): Surface morphologies of composite layers with 0 and 5 g/L lanthanum acetate; (d): Histograms of porosity and roughness

prepare the MAO composite layers. The layer thickness was measured using an optical microscope, surface hardness was measured using a digital microhardness tester (each measured five times for the average value), and morphology was analyzed using confocal microscopy. SEM was used to examine the surface and cross-sectional morphology. X-ray diffraction was used to identify the phase composition. Friction and wear tests were performed using the MS-M9000 tester under a 5 N load and 2 Hz frequency, using a 6 mm Si_3N_4 ball for 30 min in 3.5% NaCl solution (for corrosion-wear tests) and in air (for dry friction tests). Electrochemical tests were conducted using a Shanghai Chenhua 6.0 three-electrode system in 3.5% NaCl solution: OCP for 400 s; EIS from 100 kHz to 10 MHz with 0.01 V amplitude; polarization curves from −1.8 V to +0.5 V. High-resolution TEM (FEI Talos F200X G2) was used to characterize the nanoscale crystal plane structure of the worn composite layer.

3. Experimental results and analysis

3.1. Thickness, hardness, bonding force, and roughness and porosity

Fig. 1(a_1, a_2) shows cross-sectional micrographs of a composite structure featuring an Al substrate, a resin layer, and a micro-arc oxidation layer between them. Fig. 1(b) shows that incorporating 5 g/L of lanthanum acetate enhances the average hardness of the oxidation layer from 737.66 HV_1 to 1236.32 HV_1. This is attributed to the role of La in increasing electrolyte conductivity, facilitating the transformation

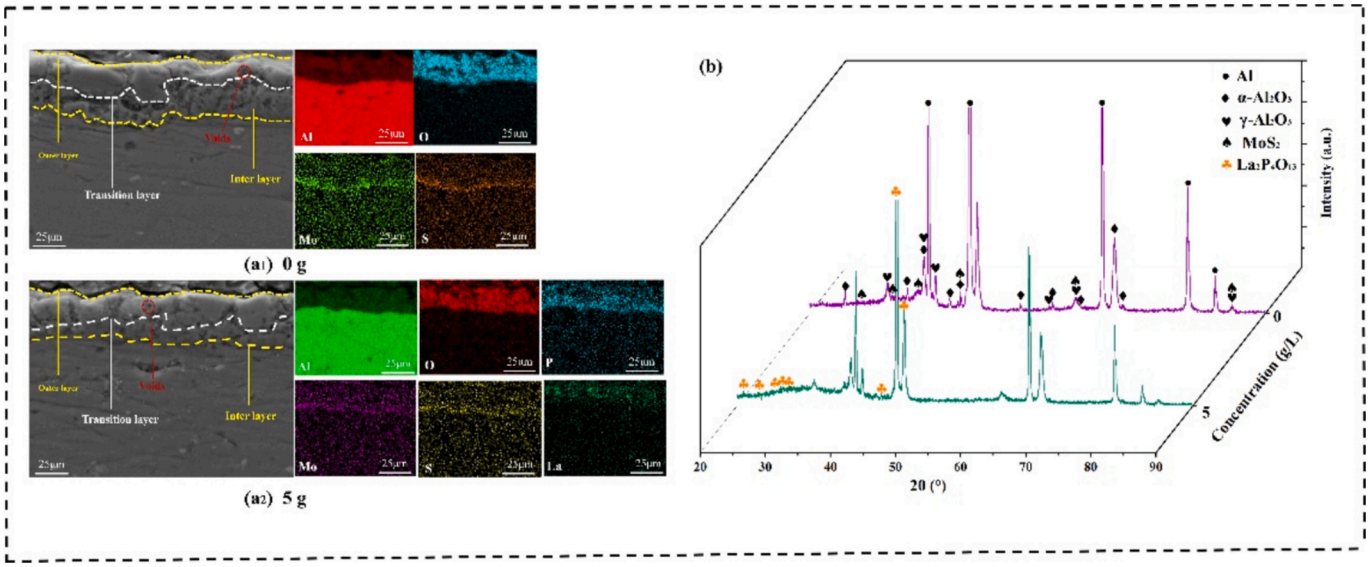

Fig. 2. (a_1): the EDS elemental distribution without the addition of lanthanum acetate;(a_2): the EDS elemental distribution with the addition of 5 g/L lanthanum acetate; (b): the XRD phase composition with 0/5 g/L lanthanum;

of γ-Al_2O_3 into the harder α-Al_2O_3, while also improving oxidation rates and discharge and make the layer be thicker. Scanning electron microscopy images (200 × magnification) of the oxide layer at varying lanthanum acetate concentrations (Fig. 1(c_1, c_2)), analyzed using Image J software to measure surface pore volume fractions, reveal that the presence of lanthanum acetate leads to a distinct self-sealing concave flake-like morphology, reduces porosity from 3.29% to 2.70%, and slightly increases surface roughness Ra. This morphological improvement contributes to the enhanced surface flatness of the composite layer.

3.2. Element and phase composition

Fig. 2(a_1) shows uniform Al, Mo, and S distribution in the composite layer at 0 g/L lanthanum acetate; P and La are uniformly distributed at 5 g/L (Fig. 2(a_2)).XRD results (Fig. 2(b)) reveal that in-situ Al_2O_3, MoS_2, and $La_2P_4O_{13}$ may form on the alloy surface as more electrolyte components participate in electrolysis: MoS_2 forms via precursor reaction (MoS_3) followed by desulfurization, while LaP_xO_y forms ($La^{3+} + MnPO_4^{(3-n)-} \rightarrow LaPO_4 + nH^+$) via a hydrothermal-like process (La salts

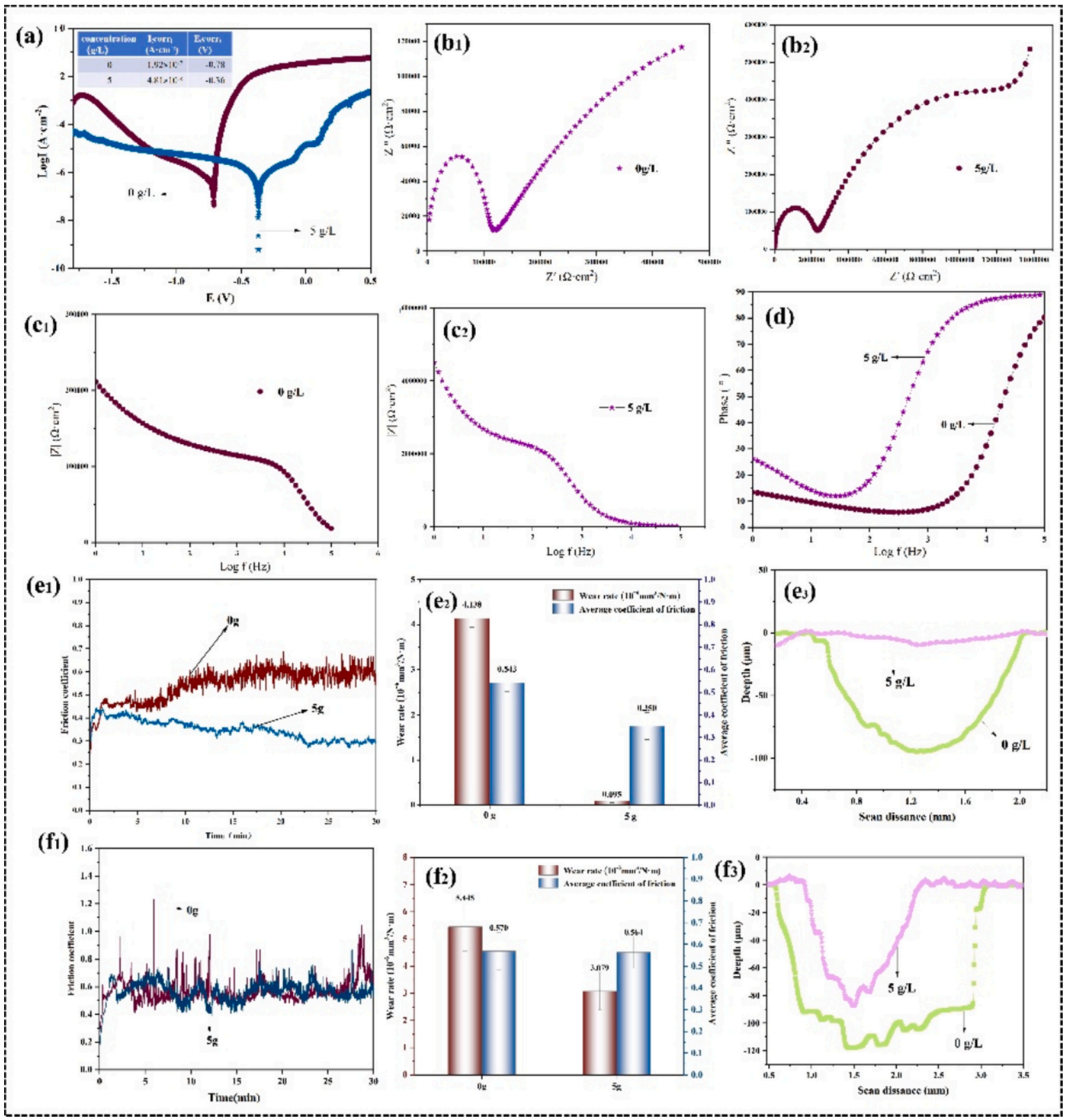

Fig. 3. Polarization and impedance spectra of composite layers at lanthanum acetate concentrations of 0 and 5 g/L; (a): Polarization curves;(b_1, b_2): Nyquist plots; (c_1, c_2): Bode plots(d): Phase-angle plots. (e_1、e_2、e_3): In 3.5% NaCl solution: friction coefficient curves、histograms of average friction coefficient and wear rate and the wear scar depth; (f_1、f_2、f_3): Under dry wear friction: coefficient curves、histograms of average friction coefficient and wear rate and the wear scar depth;

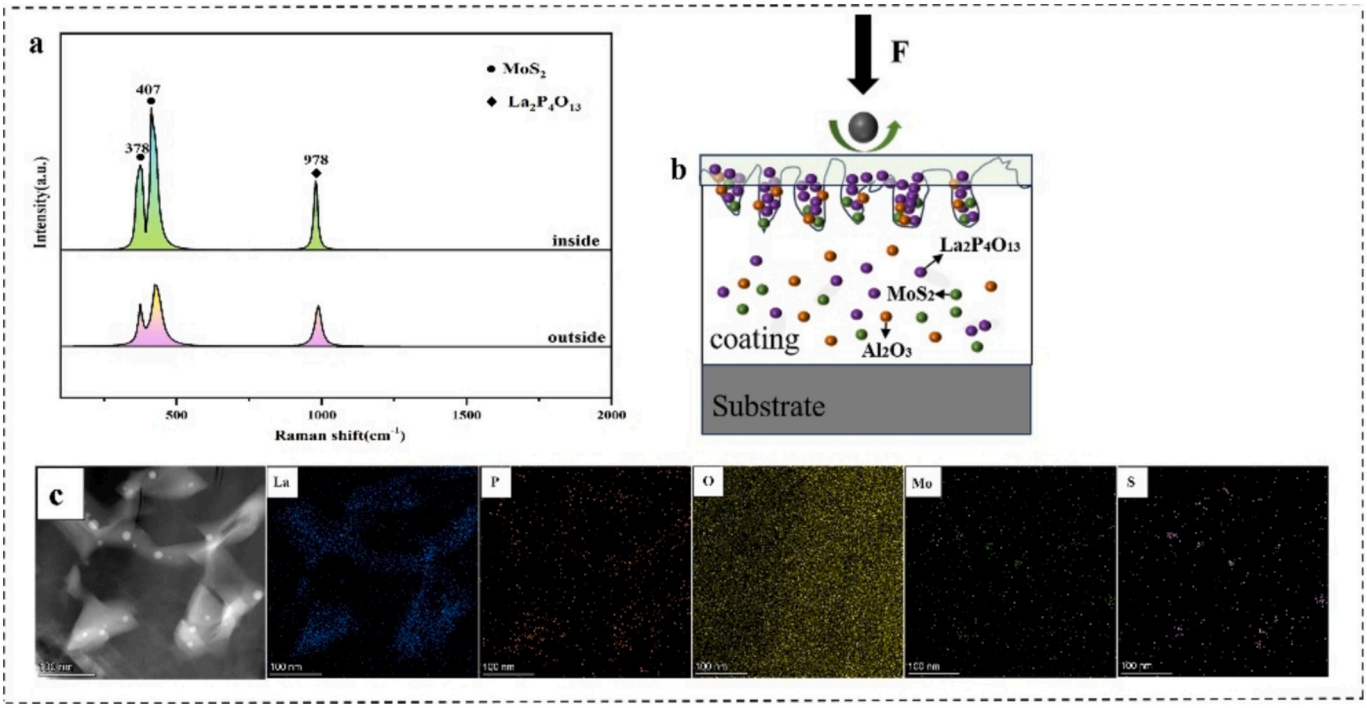

Fig. 4. (a): Raman spectra of inner/outer regions of wear scars (b)Schematic diagram of corrosion resistance and wear reduction mechanism: (c): HAADF image and mapping image.

are compatible with electrolyte additives [13]).At 0 g/L lanthanum acetate, the composite layer consists mainly of γ-Al_2O_3, α-Al_2O_3, and minor MoS_2. With lanthanum acetate addition, $La_2P_4O_{13}$ diffraction intensity increases ($2\theta \approx 26.16°$, 28.70°), and an amorphous hump (inferred as unstable rare-earth phosphate [13]) appears at $2\theta \approx 20–40°$. TEM observation.

3.3. Electrochemical and corrosion test

Electrochemical analysis (Fig. 3(a–d)) shows that the composite layer exhibits cathodic passivation (inhibiting cathodic reactions) at 0 g/L lanthanum acetate, while 5 g/L induces synergistic cathodic-anodic passivation with positive-shifted polarization potential (enhancing corrosion protective film formation). Nyquist plots (Fig. 3(b_1, b_2)) reveal the 5 g/L sample's capacitive reactance imaginary part (Z") increases by two orders of magnitude vs. the control; Bode plots (Fig. 3(c_1, c_2)) confirm a significant rise in charge transfer resistance (|Z|), and phase-angle plots (Fig. 3(d)) show its phase angle approaches 90° across frequency ranges (strong capacitive effect), confirming that 5 g/L significantly enhances the corrosion resistance of the composite layer.

In the friction test, With a 3.5% NaCl corrosion environment (Fig. 3(e_1)), the 0 g/L sample's wear scar depth exceeds layer thickness (Fig. 3(e_3)), causing failure with a friction coefficient fluctuating between 0.35 and 0.51; in contrast, 5 g/L stabilizes the coefficient at 0.34–0.41 (average 0.350) and drastically reduces volumetric wear rate from 4.138×10^{-6} to 9.5×10^{-8} $mm^3/N{\cdot}m$ (Fig. 3(e_2)). For dry wear tests (Figs. 4(f_1, f_3)), although excessive wear scar depth still leads to composite layer failure, the addition of lanthanum acetate still mitigates wear to a certain extent by exerting its strengthening and lubricating effects.

3.4. Corrosion-wear mechanism

Raman spectra (Fig. 4(a)) confirm the coexistence of MoS_2 and $La_2P_4O_{13}$ phases within the wear scar region. Mechanistically, $La_2P_4O_{13}$ enhances the corrosion resistance of the composite film by filling intrinsic micropores and cracks, which effectively blocks Cl^- ion penetration. The schematic diagram of its mechanism is shown in Fig. 4(b). Meanwhile, high-resolution structural characterization (Fig. 4(c)) reveals an incoherent Al_2O_3-$La_2P_4O_{13}$-MoS_2-$La_2P_4O_{13}$- Al_2O_3 interface structure surrounding irregular Al_2O_3 grains. Herein, in-situ formed MoS_2 nanoclusters and lamellar $La_2P_4O_{13}$ synergistically fill the intergranular pores of Al_2O_3, thereby providing critical structural reinforcement for the concurrent improvement of the composite layer's wear and corrosion resistance.

4. Conclusion

This study demonstrates that the addition of 5 g/L lanthanum acetate to the electrolyte during micro-arc oxidation enables the successful preparation of $Al_2O_3/MoS_2/La_2P_4O_{13}$ composite layers on 6082-T6 alloy, which outperforms the Al_2O_3/MoS_2 layers (with 0 g/L lanthanum acetate) in comprehensive performance. Specifically, the addition of lanthanum acetate significantly increased the hardness of the composite layer from 737 HV_1 to 1236 HV_1, reduced the porosity from 3.3% to 2.7%. Meanwhile, it enhanced the corrosion resistance of the composite layer and decreased the wear rate by two orders of magnitude, from 4.138×10^{-6} $mm^3/N{\cdot}m$ to 9.5×10^{-8} $mm^3/N{\cdot}m$. LaP_xO_y strengthens grain boundaries; MoS_2 lubricates. Together, they endow the composite layer with superior wear/corrosion resistance.

CRediT authorship contribution statement

Tao Liu: Formal analysis, Writing – original draft. **Jian Shang:** Funding acquisition, Supervision, Writing – review & editing. **Qian Li:** Data curation, Investigation.

Declaration of competing interest

The authors declare the following financial interests/personal relationships which may be considered as potential competing interests: Jian Shang reports equipment, drugs, or supplies and travel were

provided by Liao Ning Revitalization Talents Program. If there are other authors, they declare that they have no known competing financial interests or personal relationships that could have appeared to influence the work reported in this paper.

Acknowledgements

This work is funded by Liao Ning Revitalization Talents Program (XLYC2403197).

Data availability

Data will be made available on request.

References

[1] M. Zhang, X. Ma, S. Zhang, L. Hou, K.H. Kim, Surf. Coat. Technol. 497 (2025) 131796, https://doi.org/10.1016/j.surfcoat.2025.131796.
[2] S. Zhang, M. Zhang, H. Jiang, L. Chen, D. Han, X. Hu, L. Qiu, Surf. Coat. Technol. 510 (2025) 132227, https://doi.org/10.1016/j.surfcoat.2025.132227.
[3] Z.W. Li, S.C. Di, Metals 7 (4) (2017) 127, https://doi.org/10.3390/met7040127.
[4] C.Y. Du, H. Zhao, Z.Y. Dai, Z.Y. Tian, J.C. Wang, Z. Wang, Mater. Lett. 236 (2019) 723–726, https://doi.org/10.1016/j.matlet.2018.11.019.
[5] Z.L. Shao, Z.S. Ye, H.L. Lu, F.L. Fan, IEEE Trans. Power Delivery. 38 (2) (2022) 1375–1385, https://doi.org/10.1109/TPWRD.2022.3213759.
[6] E. Xue, J. Shang, F. Liu, Mater. Lett. 390 (2025) 138377, https://doi.org/10.1016/j.matlet.2025.138377.
[7] T.Y. Lin, X.Y. Zhang, X. Huang, X.P. Gong, J.J. Zhang, X.J. Hu, Rare Metals 37 (2018) 976–982, https://doi.org/10.1007/s12598-017-0948-z.
[8] D.j. Zhai, D.f. Du, H.Q. Dou, Mod. Phys. Lett. B. 33 (22) (2019) 1950265, https://doi.org/10.1142/s0217984919502658.
[9] X.Y. Lv, G.P. Zou, K. Ling, W.W. Yang, Q.F. Mo, W.Z. Li, Surf. Coat. Technol. 406 (2021) 126630, https://doi.org/10.1016/j.surfcoat.2020.126630.
[10] C.S. Ma, D. Cheng, X.H. Zhu, Z.J. Yan, J.G. Fu, J. Yu, Z.Z. Liu, S.B. Zheng, Wear 394 (2018) 109–112, https://doi.org/10.1016/j.wear.2017.10.012.
[11] Q. Li, J. Shang, T. Liu, Appl. Surf. Sci. (2025) 163353, https://doi.org/10.1016/j.apsusc.2025.163353.
[12] D.B. Marshall, P.E.D. Morgan, R.M. Housley, J. Am. Chem. Soc. 81 (1998) 951–956, https://doi.org/10.1111/j.1151-2916.1998.tb02432.x.
[13] Q. Li, J. Shang, S. Sun, Wear 568 (2025) 205968, https://doi.org/10.1016/j.wear.2025.205968.